THERMAL SHOCK RESISTANCE OF Si_3N_4-SiC MEASURED BY INDENTATION TECHNIQUE

MONIKA KAŠIAROVÁ[a], PETER TATARKO[a], JÁN DUSZA[a], MIROSLAV HNATKO[b]

[a] Institute of Materials Research, Slovak Academy of Sciences, Watsonova 47, 040 01 Košice, [b] Institute of Inorganic Chemistry, Slovak Academy of Sciences, Dúbravská cesta 9, 845 36 Bratislava, Slovak Republic
mkasiarova@imr.saske.sk, ptatarko@imr.saske.sk, jdusza@imr.saske.sk, uachmiho@savba.sk

Keywords: silicon nitride, ceramic nanocomposite, indentation, thermal shock resistance

1. Introduction

Silicon nitride is the promising materials for high temperature application because of their excellent high temperature strength, creep behaviour, oxidation and thermal shock resistance. The strong and directional covalent bonding between Si and N makes the formation of fully dense bulk materials possible only with the aid of sintering additives promoting liquid phase sintering. However, after cooling liquid phase usually retained as glassy or partially crystalline intergranular phases at three- and two- grain junctions[1,2]. At higher temperatures intergranular phases along Si_3N_4 grains soften and thus decrease the strength, creep resistance and promote oxidation. The aim of the technology is to obtain intergranular glass compositions, which are susceptible to crystallisation into a high refractory phase. It has been shown that by using rare-earth oxides as sintering additives, the high temperature mechanical properties of silicon nitride can be improved due to higher refractoriness of the residual intergranular phases[3]. The replacement of the MgO additive with Y_2O_3 or Yb_2O_3 increased the creep resistance by several orders of magnitude[4].

One of the ways of further improvement of the high temperature mechanical properties is the incorporation of SiC particles into silicon nitride matrix. The improvement of the properties is related to a change of morphology and size of grain, structure and chemistry of intergranular phase and distribution of nano-sized particles. It has been reported that when 20 % SiC was added to silicon nitride the strength of about 1000 MPa was observed at 1400 °C in air[5]. The excellent oxidation resistance for Si_3N_4–SiC nanocomposites compared with monolithic silicon nitride was reported in[6]. Creep rate of the nanocomposite is up to one order of magnitude lower than that of the reference monolithic Si_3N_4 material[7].

Components to be properly applied in high temperature need to have also high resistance to thermal shock. During thermal shock, transient thermal stresses build up in the material can become large enough to induce damage, such as microcracks or macrocracks[8] or even total failure of ceramic component/part. Due to covalent bonding Si-based ceramics such as silicon carbide and silicon nitride exhibits low thermal expansion coefficient and high thermal conductivity, and therefore a high resistance to thermal shock[9,10]. Investigation of the behaviour of Vickers indentation cracks under quenching condition has raised interest due to their simplicity to estimate thermal shock resistance. The advantage of indentation-quench method developed by Andersson and Rowcliffe[11] is easy preparation of experimental samples and small number of samples required for a series of measurements at different temperatures.

The thermal stress crack initiation and propagation behaviour of ceramics is evaluated by two thermal shock resistance parameters[12]. The resistance to initiation of crack is expressed by parameter *R*:

$$R = \sigma(1-\nu)/\alpha E = \Delta T \qquad (1)$$

where σ is the tensile strength, *E* is the Young's modulus, α is the coefficient of thermal expansion and *v* is the Poisson's ratio. Higher *R* represents a greater resistance to the initiation of fracture during rapid quenching. The second parameter is the resistance to the propagation of crack expressed by R''':

$$R''' = \left(\frac{K_{IC}}{\sigma_r}\right)^2 (1-\nu) \qquad (2)$$

which described the resistance to catastrophic crack propagation under a critical temperature difference.

The aim of this work is to study and compare the relative thermal shock resistance of two silicon nitride based materials by using an indentation quench method.

2. Experimental materials and procedure

The material was prepared by densification of Si_3N_4 / Y_2O_3 / C / SiO_2 starting mixture with weight fractions of 93.23 % / 4.91 % / 0.43 % / 1.43 %, respectively. Green discs were then embedded into a BN powder bed and positioned into the graphite uniaxial die. Samples were hot-pressed under a specific heating regime, atmosphere and mechanical pressure regime at 1750 °C and 30 MPa for 2 hours in order to produce composite with 5 wt.% of SiC particle. The *in-situ* reaction of carbon with SiO_2 in Si_3N_4 is a cheap and simple way how to produce the Si_3N_4-SiC micro-nanocomposite. The details of fabrication were published elsewhere[13]. Beside of composite material also monolithic gas pressure sintered silicon nitride with additives Al_2O_3 (3 wt.%) and Y_2O_3 (3 wt.%) was tested. Thermal shock resistance tests were performed on samples with six non-interacting Vickers indents. Bars with the dimension of 25×4×3 mm^3 surface-polished with 1 μm diamond suspension were indented by Vickers indenter at load of 98.1 N. Indents with radial cracks aligned parallel to both edges are illustrated in Fig. 1. The indented specimens were heated at predetermined temperatures in air. The temperature was held at a specified maximum for 20 min, and then specimens were quenched in water at room temperature. The lengths of radial crack, *2a*, were

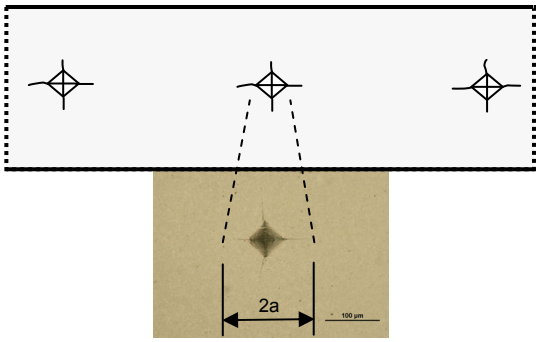

Fig. 1. **Sketch of indented sample for thermal shock resistance test**

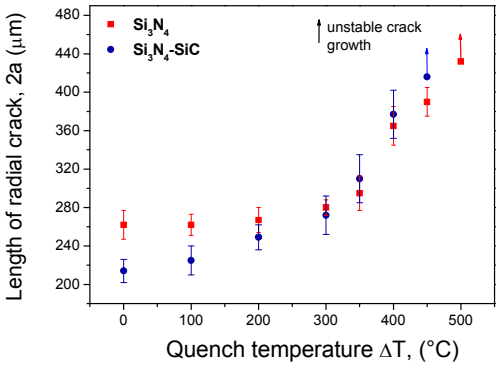

Fig. 2. **Growth of radial crack with increasing quench temperature**

measured by optical microscope. The procedure was repeated at increasing quench temperatures ΔT, up to the critical value ΔT_c at which radial crack becomes unstable and the specimen failed. Here we should point out that valid thermal shock test is only with the actual component in the condition encountered in service. Simplified test was used as a relative comparison between studied materials.

In Tab. I is summarised the basic mechanical and thermal properties of studied materials.

Table I
Some of the properties of studied materials

	Si_3N_4	Si_3N_4-SiC
Density [g/cm^3]	3.23 (99 %)	3.21 (98 %)
Young's modulus [GPa]	308 ± 14	321 ± 11
Fracture toughness [MPam$^{1/2}$]	5.80 ± 0.38	3.75 ± 0.53
4-point bend strength [MPa]	870	678
Thermal expansion coefficient 25−1200 °C [°C^{-1}]	$3.6\cdot10^{-6}$	$3.8\cdot10^{-6}$

3. Results and discussion

The experimental results of indentation thermal shock measurement are summarized in Fig. 2, where radial crack evolutions of the both ceramic materials with increasing quench temperature are shown. Despite the relatively large scatter of the data, a clear trend is observed. For both materials three different areas characterized the crack evolution after quenching were observed: I) initial insignificant growth of radial cracks with increasing ΔT (up to ΔT ~ 350 °C for Si_3N_4 and up to ΔT ~ 300 °C for Si_3N_4- SiC) is attributed to relaxation of residual indentation stresses; II) stable extension of radial crack (from ΔT ~ 350 °C to ΔT~ 400 °C for Si_3N_4-SiC and from ΔT ~ 300 °C to ΔT ~ 450 °C for Si_3N_4-SiC), regime with stable crack growth is due to the combination of thermal stresses from the quenching and residual stresses from the indent, III) unstable extension of radial crack – where the stress intensity factor at the tip of crack overcome the critical value for the catastrophic crack propagation. A critical temperature ΔT_c when the specimens failed is 500 °C for Si_3N_4 and 450 °C for Si_3N_4-SiC. Indentation crack reached instability at ΔT first in the longitudal direction (parallel to the long specimen edges). Fig. 3 shows the Vicker's indents of material Si_3N_4-SiC before quench test and after failure at quench temperature 450 °C.

From the equation (*1*) is clearly visible that the thermal shock resistance can be improved by the increase of fracture strength and by the decrease of Young's modulus and coefficient of thermal expansion. In the present investigation incorporation of the secondary phase SiC with higher elastic modulus and also thermal expansion coefficient should lead to the assumption of the lower thermal shock resistance com-

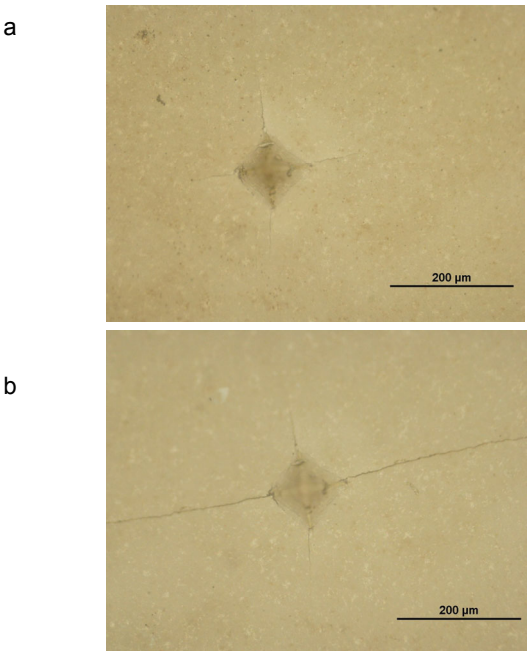

Fig. 3. **Vicker's indent of Si_3N_4-SiC before quench test a) and after quench test at 450 °C b)**

a

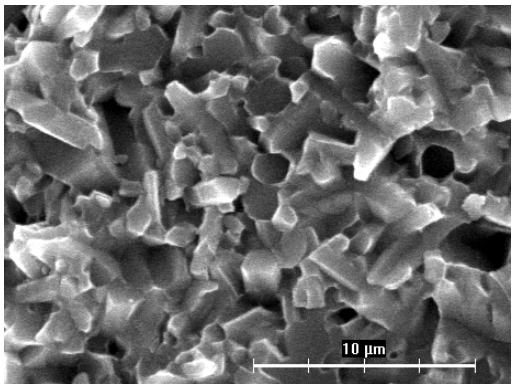

b

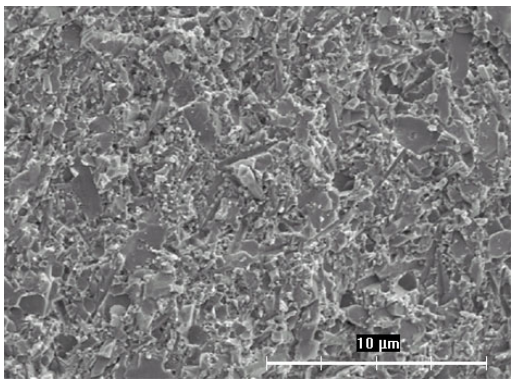

Fig. 4. **Fracture surface of monolithic silicon nitride a) and Si_3N_4-SiC composite b)**

pared to monolithic silicon nitride. If the addition of SiC leads to decrease of fracture strength (see Table I), material Si_3N_4-SiC shows decrease of the resistance to crack propagation under thermal shock.

From the length of radial crack in Fig. 1 is visible that the growth of crack in the monolithic silicon nitride is slower compare to composite Si_3N_4-SiC. This is caused by the toughening mechanisms which are active in the coarser microstructure of monolithic Si_3N_4. Fig. 4 shows the fracture surface of both studied materials. In monolithic Si_3N_4 with coarser grains pull-out and deflection were present as toughening mechanisms. Such crack bridging mechanisms are not active in the finer microstructure of nanocomposites. Present toughening mechanisms of monolithic silicon nitride enhanced the thermal shock resistance. Together with the higher strength, fracture toughness and lower Young's modulus results in better thermal shock resistance compare to composite Si_3N_4-SiC. Although the incorporation of SiC particles into silicon nitride matrix increase the creep and oxidation resistance, slight degradation of critical quench temperature and hence the resistance to thermal shock was observed.

5. Conclusions

The critical quench temperature of hot pressed composite Si_3N_4-SiC and monolithic gas pressure sintered silicon nitride was estimated. Lower thermal shock resistance of Si_3N_4-SiC is caused by the presence of SiC whose higher Young modulus and higher thermal expansion coefficient compare to Si_3N_4 degrade the thermal shock resistance. Finer microstructure of composite has also the negative influence on the indentation thermal shock resistance. In spite of theoretical consideration the experimental results show only slight (about 50 °C) decrease of value of critical quench temperature.

The work was supported by the Slovak Grant Agency project No. 2/0156/10, LPP-0203-07 and by Centrum of Excellence NANOSMART.

REFERENCES

1. Bonnell D.A., Tien T.-Y., Rühle M.: J. Am. Ceram. Soc. *70*, 460 (1987).
2. Cinibulk M. K., Thomas G., Johnson S. M.: J. Am. Ceram. Soc. *75*, 2037 (1992).
3. Gaza G. E.: Am. Ceram. Soc. Bull. *54*, 778 (1975).
4. Wiederhorn S. M.: Z. Metallkd. *90*, 1053 (1999).
5. Park H., Kim H.-E., Niihara K.: J. Eur. Ceram. Soc. *18*, 907 (1998).
6. Herrmann M., Klemm H., Göbel B., Schubert C., Hermel W.: Key Eng. Mater. *161–163*, 377 (1999).
7. Kašiarová M., Shollock B., Boccaccini A., Dusza J.: J. Am. Ceram. Soc. *92*, 439 (2009).
8. Tancret F.: J. Eur. Ceram. Soc. *26*, 1517 (2006).
9. Kalantar M., Fantozzi G.: Mater. Sci. Eng. A *472*, 237 (2008).
10. Hoffmann M. J., Schneider G. A., Petzow G.: *The Potential of Si3N4 for Shock Applications—Thermal Shock and Thermal Fatigue Behaviour of Advanced Ceramics*, s. 49. Kluwer Academic, Boston 1993.
11. Andersson T., Rowcliffe D. J.: J. Am. Ceram. Soc. *79*, 1509 (1996).
12. Hasselman D. P. H.: Am. Ceram. Soc. Bull. *49*, 1033 (1970).
13. Hnatko M., Galusek D., Šajgalík P.: J. Eur. Ceram. Soc. *24*, 189 (2004).

M. Kašiarová[a], P. Tatarko[a], J. Dusza[a], M. Hnatko[b]
(*[a] Institute of Materials Research, Slovak Academy of Sciences, Košice, [b] Institute of Inorganic Chemistry, Slovak Academy of Sciences, Bratislava, Slovak Republic*): **Thermal Shock Resistance of Si_3N_4-SiC Measured By Indentation Technique**

The critical quench temperature of composite Si_3N_4-SiC and monolithic gas pressure sintered silicon nitride was estimated by indentation technique. Work explains the decrease of thermal shock resistance of composite material compare to monolithic Si_3N_4. The degradation of composite can be attributed to the thermo-elastic properties of composite and also to the mechanical properties such as fracture toughness and strength. The refinement of microstructure makes toughening mechanisms such as crack bridging and pull-out of grain inactive and degrades the thermal shock resistance.

CHIP FORMATION PROCESS DESCRIPTION BASED ON HARD TO MACHINE ALLOYS (Ti-β AND Ni BASED)

PAWEL ROKICKI[a], ZDENEK SPOTZ[a], LENKA FUSOVA[a], KAREL SAKSL[a], CARSTEN SIEMERS[b]

[a] Slovak Academy of Sciences, Institute of Materials Research, Watsonova 47, 040 01 Kosice, Slovakia, [b] Technische Universität Braunschweig, Institut fuer Werkstoffe, Langer Kamp 8, Braunschweig, Germany
pawel.rokicki@gmail.com

Keywords: Chip formation, Shear zone, Ti-15V-3Al-3Sn-3Cr, Alloy 625

1. Introduction

Titanium and Nickel based alloys are widely used in different brunches of industry. However, machining of them is complicated due to the formation of long chips and low heat conductivity, which results in rapid tool wear. Ni based alloy 625 has constant phase constitution in range of the application temperatures[1–5].

At room temperature, pure titanium has a hexagonal close packed (hcp) structure called α-phase. At high temperature (882 °C), the hcp structure transforms to the body centre cubic (bcc) β-phase (high temperature phase). However, the room temperature stabilised β-phase due to the structural properties has much better machinability. In addition, it can be heat treated to obtain wide range of strength levels. Both of these properties allow producing products with higher accuracy at significantly lower production costs. In Ti-15V-3Al-3Sn-3Cr, a metastable β-alloy, vanadium and chromium stabilize the β-phase, whereas aluminium stabilizes the α-phase and tin is not influencing the β-transus temperature. Hence, Ti-15V-3Al-3Sn-3Cr can consist of 100 % β-phase if water quenched or air cooled from temperature above β-transus temperature[1–4,6].

Turing is a common operation in machining if rotation-symmetric parts have to be produced. During turning of Ti15V3Al3Sn3Cr and Alloy 625, long chips are produced so that the cutting operations need to be interrupted to remove the chips from the process zone. In addition, low heat conductivity of both alloys leads to rapid tool wear[1,2,4,5]. The chip formation process needs to be analysed and completely understood to design both material and machining conditions and thus to improve the machinability, leading to the reduction of the final part price.

In the present study, orthogonal cutting experiments on Ti-15V-3Al-3Sn-3Cr and Alloy 625 are performed to investigate the chip formation process.

2. Material preparation

2.1. Ti-15V-3Al-3Sn-3Cr

The Ti-15V-3Al-3Sn-3Cr alloy was prepared in the form of ingots with 7 cm diameter by GfE GESELLSCHAFT FÜR ELEKTROMETALLURGIE MbH Company. Chips from three states of materials were analyzed: as-casted state, annealed state (at 790 °C for 30 minutes and air cooled) and aged state (790 °C for 30 minutes and air cooled, 565 °C for 16 hours and air cooled).

Chips were cut orthogonally, what means that the tool had contact only with the material from which a particular chip was directly formed (Fig. 1).

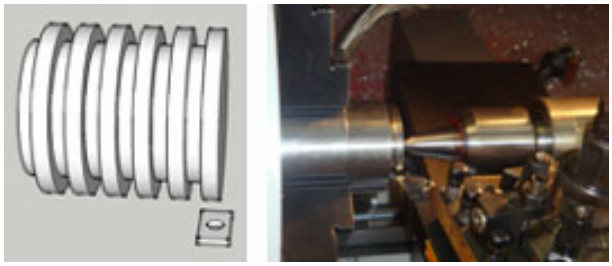

Fig.1. **Left: Visualization of ingot prepared for orthogonal cutting, Right: workstation for chips formation**

Five different speeds (10, 20, 40, 60, 80 m min^{-1}) and three depths of cut (0.05; 0.1; 0.15 mm) were used. A new tool (TiN coated) was used for every new cutting

2.2. Alloy 625

The alloy was prepared by ThyssenKrupp VDM in 7 cm diameter bars. Chips were analyzed only in as-received state. Chips were cut orthogonally (Fig. 1). Six different speeds (40, 80, 120, 160, 200, 300 m min^{-1}) and three depths of cut (0.05; 0.1; 0.15 mm) were used.

2.3. Preparation

From the obtained chips 5 to 10 mm pieces were cut and embedded at high pressure and high temperature machine. All the specimens were grinded and polished with the OPS 0.05 μm suspension mixed with H_20_2 for removal of the oxidation layer. The etching process was performed with KROLL solution. Metallographic cuts, prepared by the above procedure, were investigated by optical microscope. For scanning electron microscopy observation (Jeol JSM-7000F) the surface of each specimen was covered by thin layer of gold (few nm) to ensure conductivity and to reduce overcharging effects.

3. Results and discussion

3.1. Ti-15V-3Al-3Sn-3Cr

A cutting parameter dependent change from continuous chip formation showing a constant chip thickness to segmented chip formation process has been observed, where the single segments are separated by shear bands (inhomogeneous deformation) (Fig. 2).

Strong lines of flow are visible in the secondary shear zone, the contact area between tool and chip, in both cases. For higher cutting speeds (40 m min^{-1} and more) clear segmentation is visible. For low cutting speeds (10 and 20 m min^{-1}) there is not clearly localized deformation. The transition speed for regime change is 20–40 m min^{-1}.

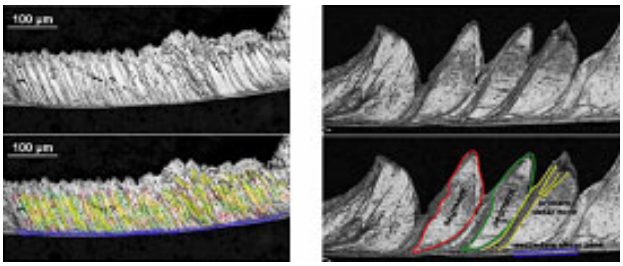

Fig. 2. **Optical microscope pictures of Ti-15V-3Al-3Sn-3Cr chips. Left: Continuous regime, Right: Segmented regime**

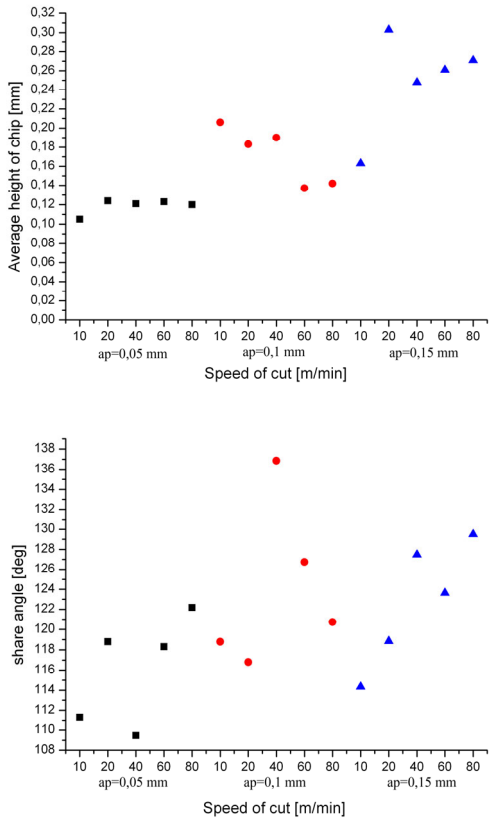

Fig. 3. **Top: Chip height in dependence of the cutting speed a strong chip compression is observed. Bottom: The shear angel increases with increasing cutting speed and depth**

Both, the average height of the chip and shear angle (angle between primary share zone and secondary share zone) were measured. Fig. 3 shows an example selected for chips from the as-received state. For the depth of cut of 0.05 mm the average height of the chip is more than 0.1 mm. Assuming that the chip is in constant volume, its compression ratio is about 200 %. Similar results are observed for cutting depths 0.1 mm and 0.15 mm. The shear angle slightly increases with increasing cutting speed, additionally, a small increase is observed with increasing depth of cut (Fig. 3, right).

Fig. 4 shows SEM pictures of shear zone. Fine microstructures in nanometer range are visible. Moreover clear border between shear zone and the segment proves that deformation occurs without influencing segment area (Formation of the shear zones is much faster that the chip formation – one does not influence the other).

Fig. 5 shows top-down view of the segments. Inhomogenity in the width of separate segments can be observed (Fig. 5, top). For heat treated states of the material this inho-

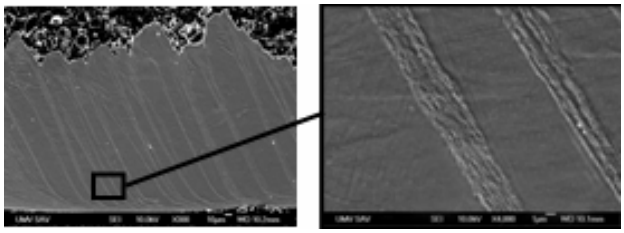

Fig. 4. **SEM picture of secondary shear zone. Fine structure in nanometer range is visible**

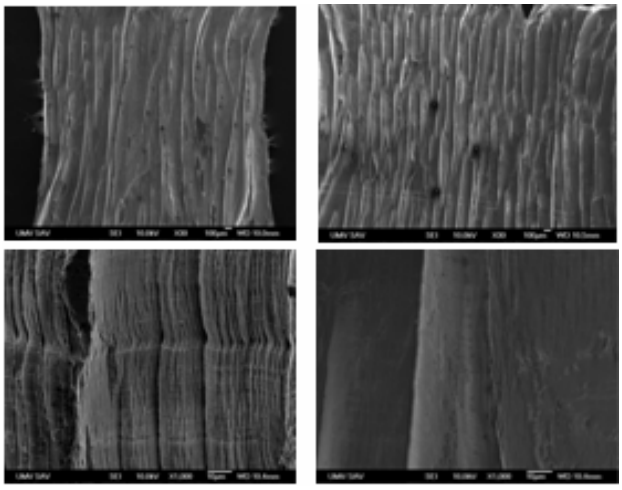

Fig. 5. **Top-down view of the chips. Top: Inhomogenity in width of separate segments on example for as-received (left) and aged (right) state. Bottom: Subsegmentation of separate segments for chips formed with low cutting speeds (left), and comparison of solid segment for high cutting speed (right)**

mogenity increases. Additionally, for low cutting speeds subsegmentation of separate segments can be observed.

3.2. Alloy 625

In case of Alloy 625 the same transition between the two main regimes is observed. For the cutting speeds from 40 to 80 m min^{-1} continuous regime is observed. For cutting speed 120 m min^{-1} and higher segmentation is visible (Fig. 6). Average height of the chips and shear angle of the Alloy 625 shows the same results as for the titanium alloy, discussed above. The width of the separate segments is also inhomogeneous.

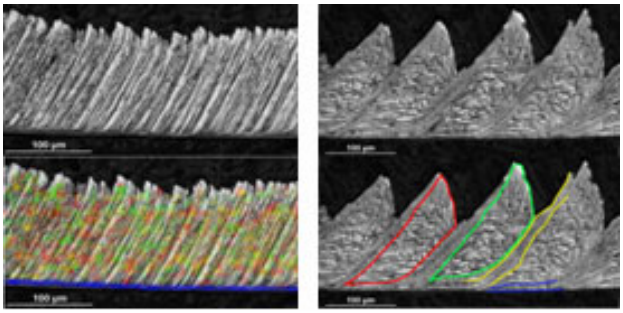

Fig. 6. **Optical microscope pictures of Alloy 625 chips. Left: Continuous regime, Right: Segmented regime**

4. Conclusions

During metal cutting of Ti-15V-3Al-3Cr-3Sn and Alloy 625 different kinds of chips are formed. Two regimes have been observed: continuous regime, in which no localized deformation is visible (homogenious deformation); and segmented regime, in which clear segments are separated by nanostructured shear zone. For Ti-15V-3Al-3Sn-3Cr, the transition speed leading to a change of chip formation mechanism was found between 20 m min^{-1} and 40 m min^{-1}. For Alloy 625 this speed is between 80 m min^{-1} and 120 m min^{-1}.

After observation of top-down view of analyzed chips, one can conclude that: The chip formation process (in orthogonal cutting) is unstable and inhomogeneous. Heat treatment (in case of titanium based alloy) increases further inhomogenity of separate segments formation.

Scanning electron microscopy proved nanometer sized grains in shear zones structure and clear border between the shear zones and the segments. Nanostructure is caused by very high deformation localized in narow shear zone followed by local rise of temperature reaching even 1000 °C through the formation[3]. Recrystalization occurs and the whole process of shear zone formation is faster than chip formation itselfs.

The research leading to these results has received funding from the European Union Seventh Framework Programme (FP7/2007-2013) under grant agreement No. PITN-GA-2008-211536, project MaMiNa. Financial support of the European Commission is therefore gratefully acknowledged.

REFERENCES

1. Boyer R., Welsch G., Collins E.W.: *Materials Properties Handbook: Titanium Alloy.* ASM INT, 1994.
2. Leyens C., Peters M.: *Titanium and Titanium Alloys – Fundamentals and Applications 2003*, Wiley-VCH, Weinheim 2003.
3. Rösler J., Bäker M., Siemers C.: *Mechanisms of Chip Formation.* (H. K. Tönshoff, F. Hollmann, ed.), Hochgeschwindigkeitsspanen, Wiley-VCH, Weinheim 2004.
4. Rokicki P.: *Analysis of high-speed machining titanium alloys.* SAS Slovakia.
5. Reed R. C.: *The Superalloys, Fundamentals and Applications.* Cambridge University Press, R.C. Reed 2006.
6 . Rokicki P., Nowag K., Spotz Z., Fusova L., Durisin J., Ghisleni R., Siemers C.: Rudy i Metale Niezelazne, *55*, 7 (2010).

P. Rokicki[a], Z. Spotz[a], L. Fusova[a], K. Saksl[a], C. Siemers[b] *([a] Slovak Academy of Sciences, Institute of Materials Research, Kosice, Slovakia, [b] Technische Universität Braunschweig, Institut fuer Werkstoffe, Braunschweig, Germany):* **Chip Formation Process Description Based on Hard to Machine Alloys (Ti-β AND Ni based)**

Titanium and Nickel based alloys, like Ti-15V-3Al-3Sn-3Cr (a precipitation hardened β-titanium alloy) and Alloy 625 are widely used in aerospace applications. Their machining, however, is difficult and expensive as their machinability is extremely poor. A thorough understanding of the chip formation process is needed to improve related metal cutting operations.

The aim of this article is to present the microstructure of Ti-15V-3Al-3Sn-3Cr and Alloy 625 chips prepared by turning. Titanium chips from different temperature states were analyzed and compared: as-received, solution treated and aged. Chips were obtained in different speeds with different depths of cut. The microstructure was analyzed by means of optical and electron microscopy. During the experiments, depending on the cutting conditions, continuous or segmented chips were formed. Narrow, highly deformed and grain oriented zone, so-called “shear zone”, separated individual segments. Different materials properties have been observed in shear zones and the segments.

The results of the chips analyses have finally been used, to develop free-machining alloys.

ANALYSIS OF MICROSTRUCTURE OF ANNEALED ALLOY Ti-15V-3Cr-3Sn-3Al AFTER DEFORMATION

ZDENEK SPOTZ[a], TONU LEEMET[b], PAWEL ROKICKI[a], LENKA FUSOVA[a], KAREL SAKSL[a] VELI-TAPANI KUOKKALA[b], CARSTEN SIEMERS[c]

[a] *Slovak Academy of Sciences, Institute of Materials Research, Watsonova 47, Kosice, Slovakia,* [b] *Tampere University of Technology, Department of Materials Science, Korkeakoulunkatu 10, Tampere, Finland,* [c] *Technische Universität Braunschweig, Institut für Werkstoffe, Langer Kamp 8, Braunschweig, Germany*
me2dd@seznam.cz

Keywords: Ti-15V-3Cr-3Sn-3Al, Deformation, Hopkinson Split Presure Bar,Hard X-Rays

1. Introduction

The Ti-15V-3Cr-3Al-3Sn alloy (or Ti-15-3) is a solute-rich β-titanium alloy, developed primarily to lower the cost of titanium sheet metal parts by reducing processing cost through the capability of being strip producible and its excellent room-temperature formability characteristics. The stabilization of β-phase is done by addition of vanadium and chromium, while aluminium is a α-phase stabilizer. In addition, aluminium, vanadium, chromium and tin as alloying elements increase the mechanical properties of the titanium alloy. Titanium alloys can also be aged to attain a wide range of strength levels to meet the requirements of a variety of applications, in many cases replacing hot-formed Ti-6Al-4V and reducing the prize of the final product[1,2].

The mechanical behaviour of materials at high strain rates differs considerably from that observed at quasi-static or intermediate strain rates. During the production of semi-finished parts, several deformation steps (e.g., rolling or forging) are necessary, leading to different microstructures and properties especially at the rod ends. The aim of this work is therefore to investigate the microstructure-property relationships of solution treated Ti-15V-3Cr-3Al-3Sn exposed to deformation at different strain rates.

2. Experiment material

For the experiments, a solute rich β-titanium Ti-15V-3Al-3Cr-3Sn was annealed at 790 °C for 30 minutes and cooled to room temperature in air. Samples of the Ti-15V-3Cr-3Al-3Sn alloy were electro discharge machined to cylinders with a diameter of 8 mm and a length of 6 mm. The specimens were deformed at three different strain rates, 10^{-3} s^{-1}, 1 s^{-1} and 10^{3} s^{-1}.

Split Hopkinson Pressure Bar (SHPB) is the most widely used technique for conducting high strain rate tests in the range of 10^{2} to 10^{4} s^{-1}. The compression test apparatus consists of two slender bars, between which the small cylindrical specimen is sandwiched. The actual test is performed by impacting a striker bar to the free end of the first (incident) bar and by the consequent travel of the elastic stress pulse through the specimen, deforming it at a high rate. For the current research, a SHPB device with Maraging steel (YS ~ 1850 MPa) pressure bars at the Department of Materials Science of Tampere University of Technology was used. Low strain rate tests were conducted on standard 100 kN servohydraulic testing machines Instron 8800 and MTS 810 (ref.[3,4]).

After the test, samples were embedded in Polyfast embedding powder (Struers) and metallographic cuts were made by the following procedure: wet grinding of the samples using silicon carbide papers with water down to grit size P2500, followed by fine polishing with diamond, particle size 1 μm, and rinsing with oil. To remove the surface oxide layer, the samples were finally polished by a mixture of OPS (grain size 0,06 μm, Sommers company) and hydrogen peroxide 2:5. Finally, the samples for metallographic observation were etched in the Kroll reagent (100 ml of H_2O, 6 ml of HNO_3, 3 ml of HF).

The general microstructures were studied by means of optical microscopy (Olympus GX 71), while the microstructural details were investigated by a scanning electron microscope (JEOL JSM LV-5600). The microstructures of deformed specimens were compared with an undeformed as-prepared sample (in figures marked as "ref"). From the micrographs the grain sizes and shapes were determined by analytical software ImageJ[5]. Hardness measurements were carried out by a Vickers hardness tester Heckert 309/54. The conditions for all hardness measurements were the same, i.e., an indentation load of 10 kg was applied for 10 seconds.

High-energy X-ray diffraction measurements were performed at HASYLAB at DESY (Hamburg, Germany) on the experimental station BW5 using monochromatic synchrotron radiation of 100.6 keV (λ = 0.12327 Å). The samples measured at room temperature were illuminated for 10 seconds by a well collimated incident beam of 1 mm^2 in cross-section. XRD patterns were recorded using a 2D detector (mar235 Image plate) in symmetric mode. The obtained XRD patterns were integrated to the scattering angle-intensity space by using the program Fit2D (ref.[6]). Phase analysis was performed by the CMPR (with database Logic)[7] and lattice parameter refinement by the PowderCell[8] computer programs.

3. Results

3.1. Optical and Electron Microscopy

The microstructures of Ti-15-3 specimens deformed at strain rates, 0.001 s^{-1}, 1 s^{-1} and 1000 s^{-1} are shown in Fig. 1 in Fig. 2. There were observed no significant changes in microstructure of specimens deformed at strain rates 0.001 s^{-1} and 1 s^{-1} compare to the undeformed state. The specimen de-

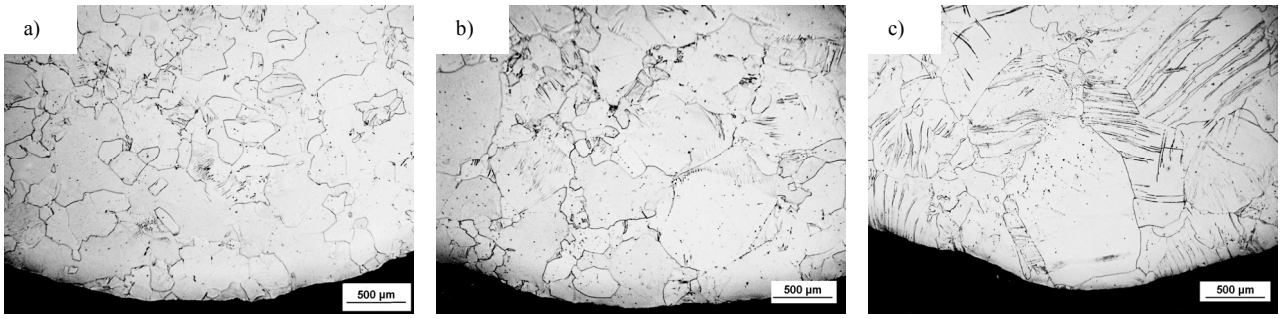

Fig. 1. **Microstructure of solution treated Ti-15-3 deformed at strain rate 0.001 s^{-1} a), 1 s^{-1} b) and 1000 s^{-1} c)**

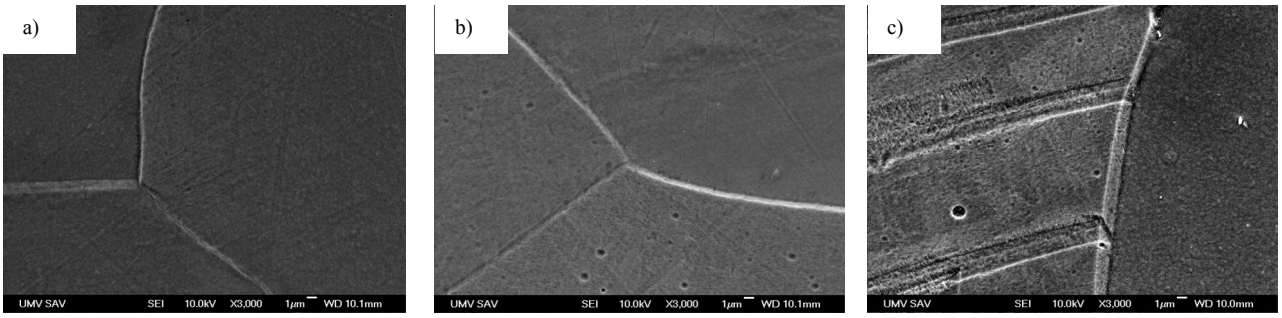

Fig. 2. **Details in the microstructure of solution treated Ti-15-3 deformed at strain rate 0.001 s^{-1} a), 1 s^{-1} b) and 1000 s^{-1} c)**

Table I
Average grain size of deformed specimens

Strain rate [s^{-1}]	undeformed	0.001	1	1000
Grain size [µm]	178	168	169	168

formed at the strain rate of 1000 s^{-1} shows significantly higher amount of deformation twins, as seen in Fig. 1c. A detailed view of the twins at a grain boundary is shown in Fig. 2c. The average grain sizes of the deformed specimens were compared with the reference sample, as shown in Tab. I. The average grain sizes of samples didn't change due to applied deformation in the range of studied strain rates.

3.2. Hardness

Tab. II shows the dependence of hardness on strain rate was observed for the specimens of Ti-15-3. No significant change in the hardness for specimens deformed within the tested range of strain rates.

Table II
Average hardness HV of deformed specimens

Strain rate [s^{-1}]	undeformed	0.001	1	1000
Hardness [HV]	278	274	268	270

3.3. X-Ray Diffraction

Fig. 3 shows the XRD patterns of tested specimens. Phase analysis proves the presence of only one phase in all samples, i.e., BCC β-Ti (S.G: Im3m). The Bragg peaks of this phase are labelled in Fig. 3. For deformed specimens of Ti-15-3 the calculated lattice parameters from the β-phase are shown in Tab. III in dependence of strain rate. For solution treated Ti-15-3 alloy the difference in lattice parameters for all deformed specimens is negligible compared to the undeformed state.

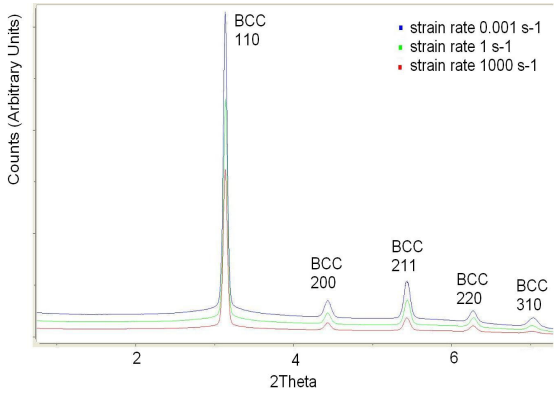

Fig. 3. **XRD patterns of deformed specimens of Ti-15-3**

Table III
Average BCC lattice parameter of deformed specimens

Strain rate [s^{-1}]	undeformed	0.001	1	1000
Lattice parameter [Å]	3.245	3.237	3.236	3.239

4. Conclusions

In this work, we have compared the microstructure of solution treated Ti-15V-3Cr-3Al-3Sn alloy after compressive deformation at strain rates ranging from 0.001 s^{-1} to 1000 s^{-1}. The samples deformed at the strain rate of 1000 s^{-1} showed significantly higher amount of twins compared to the other deformation states. The twins result from the high initial energy required for the dislocation movement at this test condition. The average grain size and shape didn't show any changes for any of the tested specimens.

Only BCC β-phase was analysed for all deformed specimens. No significant changes were observed in the lattice parameter of specimens deformed in the studied range of strain ranges compared to the undeformed material. Also the hardness values measured for all deformed specimens were similar to the undeformed state, indicating that essentially no deformation strenthening takes place in this material.

The research leading to these results has received funding from the European Union Seventh Framework Programme (FP7/2007-2013) under grant agreement No. PITN-GA-2008-211536, project MaMiNa. Financial support of the European Commission is therefore gratefully acknowledged. The hard-X-ray investigations were carried out at HASYLAB (DESY), Germany, beam line BW5.

REFERENCES

1. Boyer R., et al.: *Materials Properties Handbook-Titanium Alloys.* ASM International, 199.4
2. Smith W.: *Structure and Properties of Engineering Alloys.* (2nd ed.), McGraw-Hill, New York 1993.
3. Hokka M. et al.: *Mechanical Testing of Materials with the Hopkinson* Split Bar Technique.
4. Rämo J., Kuokkala V.-T., Vuoristo T.: J. Mater. Process. Technol. 2009.
5. Image J, software, http://rsbweb.nih.gov/ij/, actualised 2010.
6. Fit2D, software, http://www.esrf.eu/computing/ scientific/ /FIT2D/, actualised 2004.
7. CMPR and LOGIC, software and database, http:// www.ncnr.nist.gov/programs/crystallography/ /software/ cmpr/cmprdoc.html, actualised 2006.
8. PowderCell, software, ttp://www.ccp14.ac.uk/tutorial/ / powdcell/

Z. Spotz[a], T. Leemet[b] , P. Rokicki[a], L. Fusova[a], K. Saksl[a], V.-T. Kuokkala[b] , C. Siemers[c] *([a] Slovak Academy of Sciences, Institute of Materials Research, Kosice, Slovakia, [b] Tampere University of Technology, Department of Materials Science, Tampere, Finland, [c] Technische Universität Braunschweig, Institut für Werkstoffe, Braunschweig, Germany):*
Analysis of Microstructure of Annealed Alloy Ti-15V-3Cr-3Sn-3Al after Deformation

The aim of the current study is to investigate the microstructure-property relationships of solution treated Ti-15V-3Cr-3Al-3Sn exposed to deformation at different strain rates. Samples of Ti-15V-3Cr-3Al-3Sn alloy have been deformed in quasi-static and Hopkinson Split Pressure Bar experiments at strain rates between 10^{-3} s^{-1} and 10^{3} s^{-1}. The resulting microstructures were investigated by means of optical microscopy, scanning electron microscopy, and hard x-ray diffraction. In addition, the hardness of the samples was measured. The size and shape of grains were determined and compared with the undeformed state.